ISSN:1984-2295

Revista Brasileira de Geografia Física

Homepage:https://periodicos.ufpe.br/revistas/rbgfe

Assessment of desertification in the Brazilian semiarid region using time series of climatic and biophysical variables

João Guilherme Justino da Costa[1], Geber Barbosa de Albuquerque Moura[2] , Pabrício Marcos Oliveira Lopes[2], Pedro Rogério Giongo[3], José Ivaldo Barbosa de Brito[4]

[1] Ms. in Agricultural Engineering, Department of Agronomy, Federal Rural University of Pernambuco, Dom Manoel de Medeiros avenue, SN, Dois Irmãos, Recife, Pernambuco, CEP: 52171-900, Brazil, joaosabido12@gmail.com. [2] Professor Titular, Department of Agronomy, Federal Rural University of Pernambuco, Dom Manoel de Medeiros avenue, SN, Dois Irmãos, Recife, Pernambuco, CEP: 52171-900, Brazil. geber.moura@ufrpe.br. [2] Professor Associado, Department of Agronomy, Federal Rural University of Pernambuco, Dom Manoel de Medeiros avenue, SN, Dois Irmãos, Recife, Pernambuco, CEP: 52171-900, Brazil, pabricio.lopes@ufrpe.br (corresponding author). [3] Professor, Campus of Santa Helena of Goiás, State University of Goiás, Via Protestado Joaquim Bueno, No. 945 Urban Perimeter, CEP: 75920-000 - Santa Helena of Goiás, Goiás, Brazil. pedro.giongo@ueg.br. [4]Professor Titular, Academic Unit of Atmospheric Sciences. Federal University of Campina Grande, Aprígio Veloso avenue, 882 UFCG/CTRN/UACA CL Block CL room 102, Bodocongó, CEP: 58109-970, Campina Grande, Paraíba, Brazil. jivaldobrito@gmail.com.

Artigo recebido em 29/06/2023 e aceito em 12/11/2023

R E S U M O

O município de Irauçuba, localizado no Semiárido cearense, Brasil, tem enfrentado os efeitos da desertificação decorrente da escassez de chuvas. Este estudo teve como objetivo avaliar a progressão da desertificação na área de 2003 a 2020, usando dados climáticos e biofísicos coletados durante este período. Utilizamos dados complementares de estações meteorológicas automáticas operadas pela Agência Nacional de Água e Saneamento Básico para determinar o índice de anomalia pluviométrica da série histórica. Além disso, realizamos a validação de escala anual dos dados do CHIRPS usando indicadores estatísticos, como coeficiente de correlação de Pearson, erro médio, viés percentual e raiz quadrada do erro médio. Posteriormente, analisamos as mudanças de cobertura e uso da terra ao longo de 17 anos (2003-2020) no município por meio do processamento de dados CHIRPS, produto MODIS (MOD16A2 e MOD11A2) e MapBiomas na plataforma digital Google Earth Engine e software QGIS. Analisamos as mudanças de cobertura e uso da terra usando dados do MapBiomas. Finalmente, analisamos o índice de aridez para o mesmo período de 17 anos. Os resultados da pesquisa revelaram uma correlação significativa entre a precipitação pluvial e os parâmetros biofísicos, com o menor índice de aridez de 0,255 observado entre 2012 e 2014 e o maior de 0,464 entre 2018 e 2020. A suscetibilidade da área ao processo de desertificação foi classificada como alta, o que é consistente com o clima Semiárido da região. A metodologia empregada durante a pesquisa mostrou ser uma tecnologia sustentável de baixo custo econômico, reveladora e de fácil acesso, o que possibilitou a criação de uma contribuição científica para futuros trabalhos na região, além de poder agregar conhecimento para estudos de degradação ambiental.

Palavras-chave: MapBiomas, índice de anomalias pluviométricas, MODIS, CHIRPS, índice de aridez, Google Earth Engine.

Assessment of Desertification in the Brazilian Semiarid Region using Time Series of Climatic and Biophysical Variables

A B S T R A C T

The municipality of Irauçuba, located in the Semiarid region of Ceará, Brazil, has faced the effects of desertification resulting from the scarcity of rainfall. This study aimed to assess the progression of desertification in the area from 2003 to 2020, using climatic and biophysical data collected during this period. We used supplementary data from automatic meteorological stations operated by the National Agency of Water and Basic Sanitation to determine the rainfall anomaly index of the historical series. Additionally, we performed annual scale validation of the CHIRPS data using statistical indicators such as Pearson Correlation Coefficient, Mean Error, Percentage BIAS, and Root Mean Square Error. Subsequently, we analyzed land cover and land use changes over the 17 years (2003-2020) in the municipality by processing CHIRPS, MODIS product (MOD16A2 and MOD11A2), and MapBiomas data in the Google Earth Engine digital platform and QGIS software. We analyzed land cover and land use changes using MapBiomas data. Finally, we analyzed the aridity index for the same 17-year period. The research findings revealed a significant correlation between rainfall and biophysical parameters, with the lowest aridity index of 0.255 observed between 2012 and 2014 and the highest of 0.464 between 2018 and 2020. The area's susceptibility to the desertification process was classified as high,

which is consistent with the Semiarid climate of the region. The methodology employed during the research proved to be a sustainable technology of low economic cost and telling and easy access, which enabled the creation of a scientific contribution for future works in the region, besides being able to add knowledge for studies of environmental degradation.
Keywords: MapBiomas, rainfall anomaly index, MODIS, CHIRPS, aridity index, Google Earth Engine.

Introduction

The exploitation of natural resources has gone hand in hand with the advance of industrialization, and this dynamic has generated a greater demand for raw materials, implying head pressure on the environment, resulting in the Earth's surface constantly changing (Silva et al., 2021). Based on this information, it is clear that agriculture is one of the activities that most impact the environment due to human actions, such as deforestation without criteria, fires, and the excessive practice of grazing animals in areas with high fragility (Anache et al., 2017). The constant use of these human actions directly reflects on the characteristics of ecosystems, such as biodiversity losses resulting from profound changes in habitat, acceleration of erosion processes, and decline in soil fertility, which over time, the set of these factors gives rise to a degradation process (Qian et al., 2017; Shah et al., 2017; Pereira et al., 2020).

Furthermore, the Brazilian semiarid region represents a challenge for increasing productivity given its unique climatic and biophysical characteristics. These areas often experience irregularly distributed rainfall both in space and time, which can be unpredictable, leading to reduced water availability and high evapotranspiration potential. Additionally, the region is characterized by low soil fertility and constant anthropic pressures on the environment, as highlighted by Costa et al. (2020). The combination of climate variations and human activities in the region contributes to a process known as desertification, a global problem that affects the arid, semiarid, and dry sub-humid climate regions of the Earth, as described by Vieira et al. (2015), Mariano et al. (2018).

In 2010, the National Plan to Combat Desertification (PNCD) identified that the majority of land susceptible to desertification in Brazil located in the Semiarid area of the Northeast region, with approximately 181,000 km² covering 1,488 municipalities across nine states currently undergoing desertification (Perez-Marin et al., 2013; Sampaio et al., 2020). Four areas in the Brazilian Semiarid region are considered desertification nuclei: Gilbués (Piauí), Irauçuba (Ceará), Seridó (Rio Grande do Norte), and Cabrobó (Pernambuco) (Soares et al., 2011). Notably, the Irauçuba nucleus in the northwest of Ceará state deserves special attention due to the marked condition of desertification in the municipality caused by low rainfall (Landim et al., 2011).

In recent years, remote sensing techniques can detect and help monitor areas at risk or susceptible to desertification. Remote sensing provides information quickly and without direct contact with the object of study, being an alternative to the high costs of field and laboratory work to collect primary data (Xu et al., 2009; Ma et al., 2011; Passos et al., 2013; Joseph et al., 2018; Mao et al., 2018; Pacheco, 2018; Wunder and Bodle, 2019).

Remote sensing has enabled the spatial and temporal assessment of desertification processes, increasingly using climatic data and environmental components such as vegetation indices (Normalized Difference Vegetation Index - NDVI, Soil Adjusted Vegetation Index - SAVI, Leaf Area Index - LAI) and biophysical parameters (surface albedo, soil temperature, rainfall, and daily evapotranspiration) (Cunha et al., 2020; Rodrigues et al., 2020; Silva et al., 2020a; Oliveira Júnior et al., 2023; Sousa et al., 2023; Neto et al., 2023).
In the literature, it is possible to find research on the application of remote sensing in the municipality of Irauçuba to identify areas at risk of desertification (Santos et al., 2014; Oliveira et al., 2017). However, there is still a scarcity of methodologies that evaluate these environmental changes in the long term to correlate the influence of each parameter individually (Schulz et al., 2017). Monitoring environmental changes is essential to help effective public policies aimed at managing natural resources in affected areas, as highlighted by Ayele et al. (2018). Additionally, according to Pereira et al. (2017), few studies address the annual seasonality of degradation, particularly in a quantitative scope, and this information is of great importance for areas with long periods of drought.

Bohn et al. (2020) conducted a study to identify areas at risk of desertification in Rio de

Janeiro, using the Thornthwaite aridity index and the Hare (1983) D-index. The utilization of the Thornthwaite aridity index identified 5.35 times more areas susceptible to desertification than the D index method. Similarly, Santos et al. (2022) conducted a study in the Southeast region of Brazil and found no areas at risk of desertification when using the D index.

This study aimed to assess the desertification process in the municipality of Irauçuba, Ceará, using climatic and biophysical data from the Climate Hazards Group InfraRed Precipitation with Station data (CHIRPS) and the Moderate Resolution Imaging Spectroradiometer (MODIS) products, along with Google Earth Engine (GEE) virtual processing, over 17 years (from 2003 to 2020). In addition, the Precipitation Anomaly Index and the Aridity Index classified the years into dry, regular, and rainy and the level of susceptibility to desertification, respectively.

Material and methods

The study area was the municipality of Irauçuba, located in the Semiarid region of Northeastern Brazil in the state of Ceará. Situated in the micro-region of Sobral, it is 146 km from the capital, Fortaleza. Irauçuba has a Semiarid tropical climate, classified as BSh according to the Köppen-Geiger climate classification system. The average annual rainfall in Irauçuba for 2020 was 898 mm, with a historical average of 463 mm, making it one of the areas with the lowest average rainfall in the state of Ceará, according to the Institute of Research and Economic Strategy of Ceará (IPECE, 2016). The municipality's coordinates range from latitudes 3°36'00" S to 4°12'00" S and longitudes 39°24'00" W to 40°12'00" W (Figure 1).

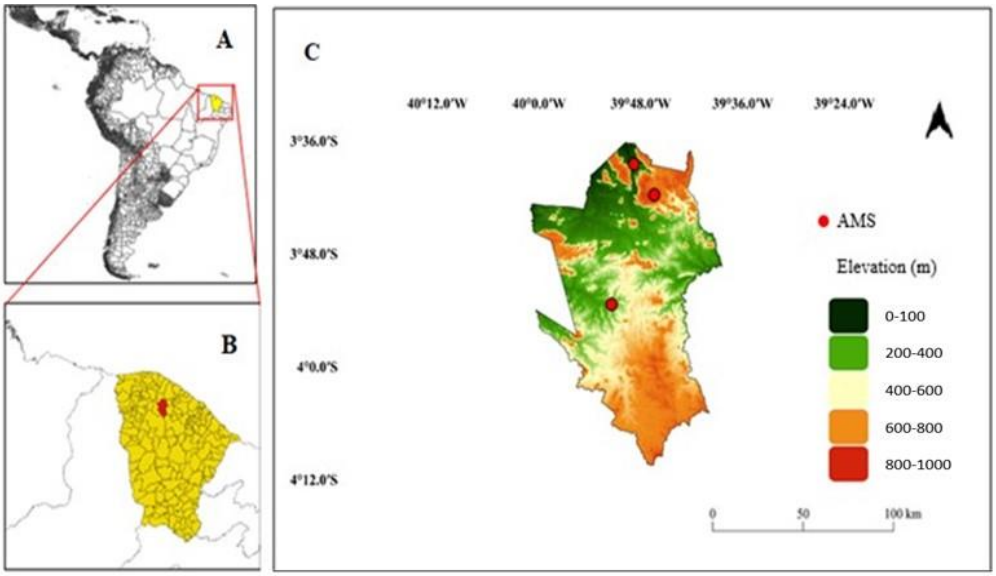

Figure 1. Spatial location of the municipality of Irauçuba, Ceará, Brazil.

The predominant natural vegetation in the study area is the Open Shrubby Caatinga, which is restricted in surface area and commonly found in shallow sandy or gravelly soils that experience long dry periods (Prado, 2003). The characteristic grounds of the region include Noncalcic Bruno, Litholic Soils, Solodic Planosolo, and Red-Yellow Podzolic. Cattle raising is practiced throughout the Planossolos and Luvissolos, while agriculture and timber extraction occur in smaller portions of the Luvissolos and Litolics. The predominant relief in the study area's geomorphology presents Sertanejo Depressions and Residual Massifs (IPECE, 2016).

The rainfall data, collected from the network of Automatic Meteorological Stations (AWS) of the National Agency for Water and Basic Sanitation (ANA) and available through the website http://www.snirh.gov.br/hidroweb, covering the period from 2003 to 2020 and was maintained by the Institute of Meteorology and Water Resources of Ceará (FUNCEME). Annual rainfall totals validated CHIRPS estimates. Table 1 presents the stations used, while Figure 1 shows their spatial distribution.

Table 1. List of Automatic Weather Stations (AWS) used in the study. Source: ANA: http://www.snirh.gov.br/hidroweb.

Codes	Weather Stations	Lat. (°)	Long. (°)	Elevation (m)	Failures (%)
339055	Missi	- 03° 37’	-39° 49’	99	30.09
339054	Juá	- 03° 52’	-39° 53’	180	5.09
339053	Irauçuba	- 03° 44’	-39° 47’	190	2.78

As observed in Table 1, the data obtained from the selected AWS exhibit a notably high percentage of failures, particularly in Missi. Therefore, it is necessary to employ techniques for filling in missing rainfall data.

The filling technique utilized was the Regional Weighting Method (Equation 1) as per the methodology established by Ruezzene et al. (2020). This method is relatively straightforward by Silva et al. (2017) as it fills in the missing data through a weighting process based on information from a minimum of three neighboring stations within the climatological region that matches the location of the study point.

$$y = \frac{1}{n}\left[\frac{x_1}{xm_1} + \frac{x_2}{xm_2} + \frac{x_3}{xm_3} + \cdots + \frac{x_n}{xm_n}\right] \quad (1)$$

where: y represents the mean annual rainfall value to be estimated (the failure to fill in); n represents the number of neighboring stations used for the estimation process; x1, x2, x3 represent the observed average annual rainfall values in the neighboring stations for the year estimated; xm1, xm2, xm3 represent the average precipitation totals at nearby stations for all available years.

Then, the Double Mass test checked the consistency of the filled rainfall data (Junqueira et al., 2018). According to Oliveira et al. (2021), the filled historical series rainfall data should be proportional to the average values of the control variable, in which case the neighboring station readings and the points should align along a straight line.

The digital procedure of the satellite images executed in the GEE platform (https://code.earthengine.google.com/) and in the QGIS software (version 3.18.3 - Zürich) involved the steps: pre-processing of the digital data, analysis of the interaction between the biophysical parameters and the degradation process of the land and the use of the soil; and elaboration of annual thematic degradation maps of the municipality of Irauçuba in the period from 2003 to 2020.

CHIRPS rainfall, potential evapotranspiration (PET), and surface temperature (LST) images from the MODIS products (MOD11A2 and MOD16A2) were scaled to 500 m to ensure spatial consistency. This homogenization of orbital data helped to minimize possible processing errors that may have occurred during the study.

Then, the GEE platform calculated the arithmetic mean of the LST and NDVI data using the (.mean) command. This operation aimed to obtain an average value for each biophysical parameter per year. Similarly, the total annual PET value was obtained by summing the PET data using the (.sum) command. To make the analysis of biophysical parameters easier during the study period, we simplified the data through various operations.

The MapBiomas platform (https://mapbiomas.org) provides thematic maps of land use and land cover for the municipality of Irauçuba for the period from 2003 to 2020. These orbital products identify areas susceptible to desertification, making it possible to infer changes in land use and land cover in this time interval. In QGIS software, the Raster tool extracted the spectral bands for each year and quantified land use and land cover areas based on image pixel size. Three-year average images of biophysical parameters evaluated the temporal evolution of environmental changes in the study area.

The statistical parameters Pearson's correlation coefficient (r), Mean Error (ME), Percentage Bias (PB), and the Square Root of Mean Error (SRME) assessed the accuracy of CHIRPS data (Silva et al. 2017, Costa et al. 2019 and Oliveira et al. 2021).

The coefficient r relates the precipitation data measured at Automatic Weather Stations (AMS) and the estimated CHIRPS. The r values vary from -1 to 1, with perfect correlation indicated by the value 1 (Silva et al. 2017, Oliveira et al. 2021).

The ME represents the mean difference between estimated CHIRPS rainfall data and those

measured at an AMS expressed by Equation 2 (Silva et al. 2020b, Nawaz et al. 2021):

$$ME = \frac{\sum(C-E)}{N} \quad (2)$$

The BP measures the systematic difference between the CHIRPS rainfall estimate and measurements from an automatic meteorological station, used to assess whether there is a perfect correlation equal to zero, underestimation for negative values, or overestimation for positive ones (Costa et al. 2019, Silva et al. 2020b) expressed by Equation 3:

$$BP = 100 * \frac{\sum(C-E)}{\sum E} \quad (3)$$

where: C is the estimated rainfall data from CHIRPS; E is the observed rainfall data from AMS; N is the total number of sample points.

RSME represents the standard deviation of the difference between automatic weather station measurements and CHIRPS product precipitation estimates (Paca et al. 2020, Nawaz et al. 2021, Hsu et al. 2021).

The biophysical parameters of Evapotranspiration, Surface Temperature, and NDVI were analyzed using descriptive statistics in QGIS. Central tendency (mean) and dispersion estimates include maximum and minimum values and standard deviation (SD). Biophysical parameters and CHIRPS rainfall were analyzed using the correlation coefficient and determination coefficient (R^2) method proposed by Guilherme et al. (2022). The analyzed pairs were: LST x NDVI, LST x CHIRPS, and NDVI x CHIRPS.

The Rainfall Anomaly Index (RAI), proposed by Van Rooy (1965), is a simple and effective index that compares rainfall anomalies in different regions. Equations 4A for positive anomalies and 4B for negative anomalies calculate the regular condition rainfall anomalies.

$$RAI = +3\frac{(P-Pmed)}{(Pmax-Pmed)} \quad (4A)$$

$$RAI = -3\frac{(P-Pmed)}{(Pmin-Pmed)} \quad (4B)$$

where: P is the current annual rainfall (mm); Pmed is average value of total annual rainfall in the historical series (mm); Pmax are average rainfall values for the ten largest annuals in the historical series (mm); Pmin are average rainfall values of the ten lowest annual historical series (mm).

The technique for monitoring the spatial-temporal variation of rainfall in a region considers that rainfall distribution follows a normal distribution. This technique characterizes and monitors rainfall deviations or anomalies in a given season, allowing comparisons between current observation conditions and historical rainfall values. In addition, this technique evaluates the spatial distribution of the rainfall event based on its intensity, showing effectiveness for semiarid locations.

After using this technique to obtain data, the values of rainfall anomalies are labeled according to Table 2 by Van Rooy (1965). However, without further context, not clear what this classification implies or how it relates to monitoring rainfall variability.

Table 2. Rainfall Anomaly Index (RAI) classes.

RAI Ranges	Classes
RAI > 4	Extremely Rainy
2 < RAI ≤ 4	Very Rainy
0 < RAI ≤ 2	Rainy
RAI = 0	Normal
-2 < RAI < 0	Dry
-4 < RAI ≤ -2	Very Dry
RAI ≤ -4	Extremely Dry

An Excel table included information about the average value of total annual rainfall and reference evapotranspiration to calculate the aridity index. The United Nations Environment Program (UNEP, 1992) proposed Equation 5 to express the degree of aridity in arid or semiarid areas given by:

$$AI = \frac{P}{ETo} \quad (5)$$

where: AI represents the aridity index, P represents the average annual rainfall, and ETo represents the reference evapotranspiration.

An aridity index is a valuable tool for assessing the degree of aridity in a given area, as it reflects the balance between water supply and demand at the surface level. Following the equation proposed by the UNEP, the aridity index values were obtained and interpreted according to the

methodology proposed by Vilar and Medeiros (2019), which likely involved specific criteria for classifying regions as arid, semiarid, or non-arid based on the calculated values.

The climate classification considers the guidelines of Resolution No. 238 of the National Council for the Environment (CONAMA) and desertification susceptibility assessed with the National Plan to Combat Desertification, including three categories that vary according to the aridity index. These categories, as illustrated in Tables 3 and 4 of the work by Matallo Junior (2001), are relevant for understanding the environmental conditions and potential risks in the study area.

Desertification risk level refers to the degree of susceptibility of an area to desertification, which is the process of land degradation in arid, semi-arid, and dry sub-humid regions (Table 4). The risk of desertification depends on natural and human factors such as climate variability, land use practices, and population pressure.

Areas with a high risk of desertification have soil erosion, reduced vegetation cover, and water scarcity, leading to biodiversity loss, decreased agricultural productivity, and increased poverty (Vieira et al., 2015; Silva et al., 2020c).

Table 3. Climate classification considering the Aridity Index.

AI Ranges	Classes
$AI \leq 0.03$	Hyperarid (H)
$0.03 < AI \leq 0.2$	Arid (A)
$0.2 < AI \leq 0.5$	Semiarid (SA)
$0.5 < AI \leq 0.65$	Subhumid dry (SUS)
$0.65 < AI \leq 1.0$	Subhumid (SU)
$AI > 1.0$	Humid (U)

Source: Adapted from Matallo Júnior (2001).

Table 4. Desertification risk classes from the Aridity Index.

AI Ranges	Desertification risk level
$AI < 0.05$	Less than Very High (LVH)
0.05 – 0.20	Very High (VH)
0.21 – 0.50	High (H)
0.51 – 0.65	Moderate (M)
$AI > 0.65$	Above Moderate (AM)

Source: Adapted from Matallo Júnior (2001).

Results and discussion

After the failure filling step, we obtain a comprehensive set of average values for total annual rainfall data in the municipality of Irauçuba from 2003 to 2020. This database served as a relevant representation of the rainfall patterns and regimes in Irauçuba in the specified period. These values can identify trends, analyze the impact of climate change, and help inform decisions related to water management and agricultural planning in the region.

Figure 2 and Table 5 present the descriptive statistics of annual rainfall totals at the weather stations in Missi, Juá, and Irauçuba over the 17-year study period, with the highest average value of 1310 mm observed in 2009. The series exhibited a maximum rainfall of 1756 mm in 2009 and a minimum of 146 mm in 2012. The standard deviation ranged from 14 to 387. These findings are consistent with Mâcedo and Oliveira Santos (2021) characterization of maximum rainfall events in Forquilha, another municipality in the northeastern Semiarid region, where they identified one of the highest rainfall rates in 2009 and noted the region's susceptibility to anomaly events. These results agree with Lima et al. (2022), who reported the highest average in 2009 and the lowest in 2012.

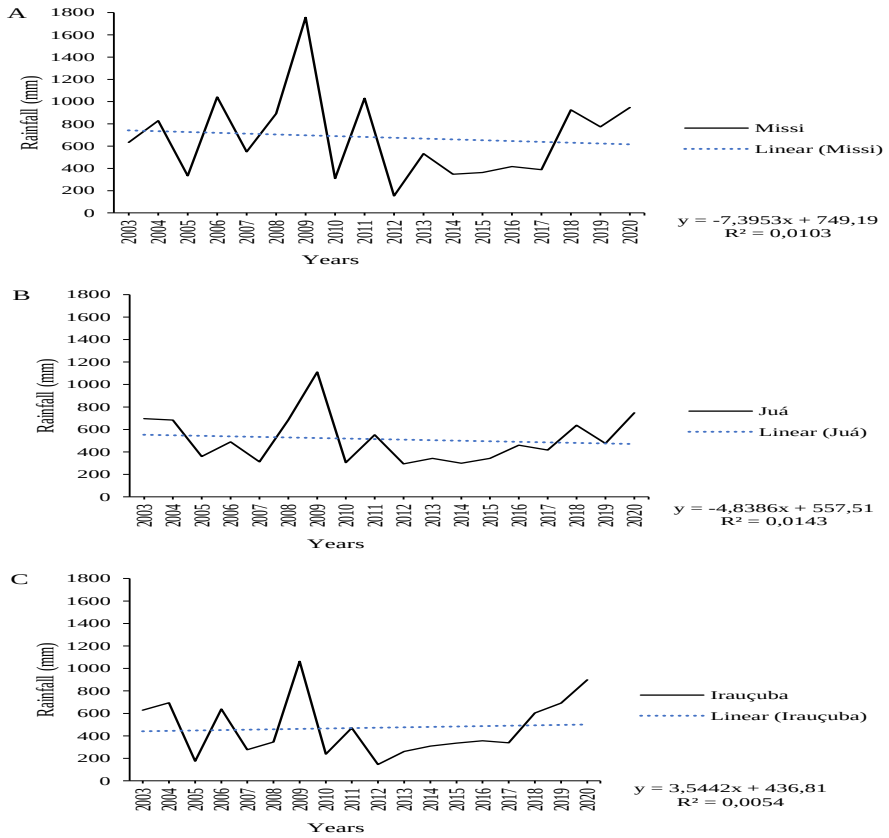

Figure 2: Annual rainfall totals for the period 2003 to 2020, with data from the Missi (A), Juá (B), and Irauçuba (C) stations, linear trend line, and standard deviation of the series. Source: Own.

Table 5: Mean, maximum (Max), minimum (Min) values and standard deviation (SD) of annual rainfall totals from the AMS (Missi, Juá, and Irauçuba) for the historical series. Source: Own.

.Years	Mean	Max	Min	SD
2003	653	697	629	38
2004	736	829	683	81
2005	289	359	175	100
2006	724	1042	489	286
2007	379	549	277	148
2008	641	892	345	276
2009	1310	1756	1063	387
2010	284	310	237	41
2011	684	1030	471	302
2012	197	294	146	84
2013	378	532	261	139
2014	319	347	299	25
2015	347	363	335	14
2016	411	461	357	52
2017	381	417	338	40
2018	723	926	604	177
2019	647	773	475	154
2020	864	947	748	104

The RAI is a measure used to assess deviations in rainfall patterns from the long-term average. Positive RAI values indicate higher-than-average rainfall, while negative values indicate lower-than-average rainfall.

In Figure 3, we can observe the RAI values for the municipality of Irauçuba between 2003 and 2020, with positive values indicating rainfall above average and negative values indicating rainfall below average. For years 2003, 2004, 2006, 2009, 2018, 2019, and 2020 showed positive RAI values, while 2005, 2007, 2008, 2010, 2011, 2012, 2013, 2014, 2015, 2016, and 2017 showed negative RAI values. It is worth noting that Landim, Silva, and Almeida (2011) and Santos et al. (2014) obtained similar patterns of RAI values for the years 2003 to 2008 in their evaluation of the rainfall anomaly index in the municipality of Irauçuba between 1981 and 2008.

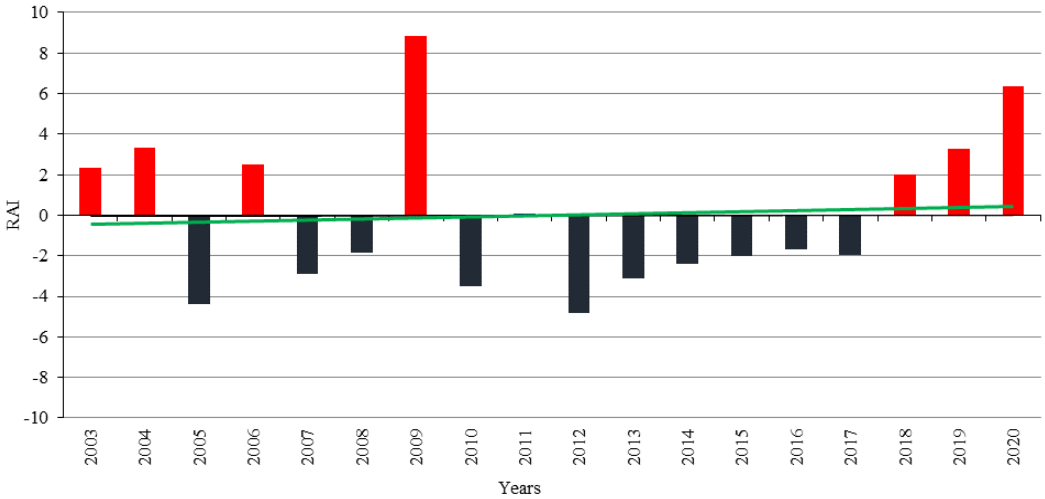

Figure 3. Index of Positive and Negative (RAI) for the annual totals of Missi, Juá and Irauçuba, from 2003 to 2020. Source: Own.

For years 2010, 2015, and 2016, negative RAI anomalies coincided with periods of drought (Table 6). In the last three years of the analyzed series (2018, 2019, and 2020), the RAI classification was positive, following eight years of negative RAI (2010 to 2017). Before this period, there was an alternation in the intensity of the periods classified as dry and rainy (Figure 3). Landim et al. (2011) noted the impact of climate variability on rainfall variability in Irauçuba, classifying the region as temporally irregular with low rainfall values. Silva et al. (2017) have reported that climatic events can cause significant changes in the rainfall regime, which may result in severe droughts depending on their intensity. This phenomenon is observed between 2010 and 2017, as shown in Figure 3, showing a strong correlation with the absence of rainfall in Northeast Brazil from 2012 to 2017. In addition, Table 6 presents the RAI classification of annual rainfall totals for the municipality of Iraucuba.

Table 6. Classification of dry, regular, and rainy years according to the RAI for Mossoró, Juá, and Irauçuba. Source: Own.

Years	Classification
2009, 2020	Extremely Rainy
2003, 2004, 2006, 2019	Very Rainy
2018	Rainy
2011	Regular
2008, 2015, 2016, 2017	Dry
2007, 2010, 2013, 2014	Very Dry
2005, 2012	Extremely Dry

Figure 4 and Table 7 illustrate the results between rainfall data from CHIRPS and those observed in Missi, Juá, and Irauçuba. The best estimate of rainfall data was for Irauçuba (Figure 4C), where the point clouds followed the trend line. The Pearson correlation coefficients demonstrate that Irauçuba had the highest correlation (0.90) between rainfall data from CHIRPS and those observed in the station. Juá station also showed a good correlation (0.84), while the Missi station had the lowest correlation (0.82). These results align with those reported by Paredes-Trejo et al. (2017), who found high to nearly perfect monthly correlation coefficients (r ranging from 0.87 to 0.93) for the Caatinga biome region.

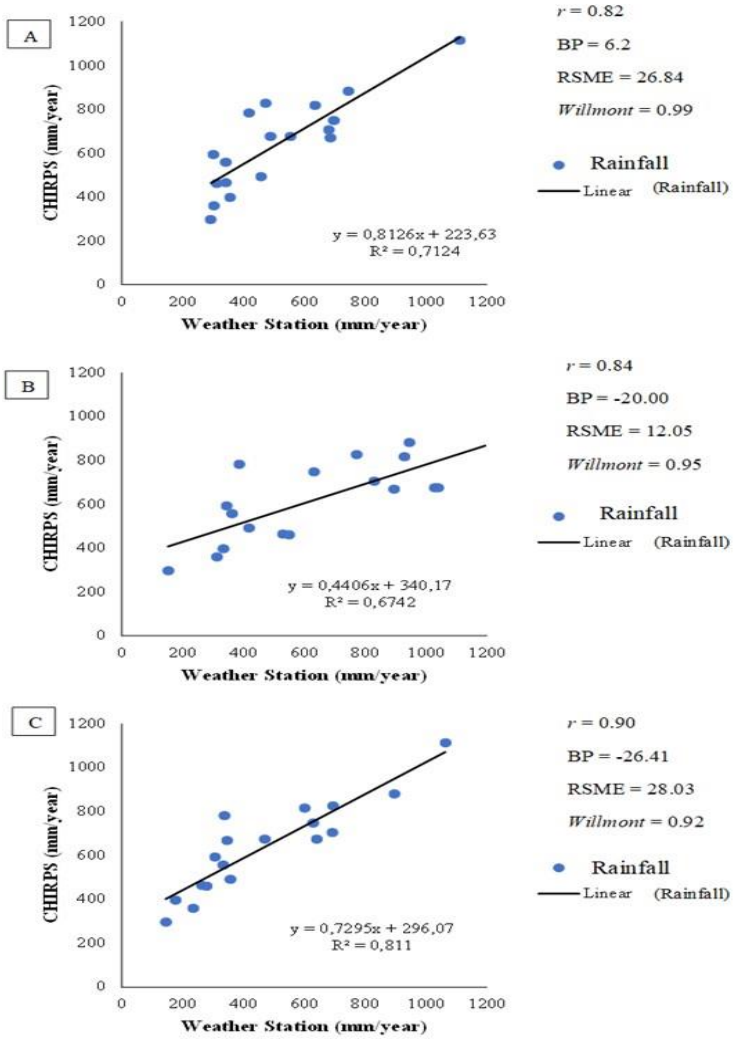

Figure 4. Comparison between measured and estimated rainfall using CHIRPS for the following locations: Missi (A), Juá (B), and Irauçuba (C). Source: Own.

The CHIRPS data (Table 7) demonstrated strong performance in detecting rainfall distribution, evidenced by the percent BIAS values ranging from -20.0% to 6.2%. However, the CHIRPS data showed overestimation for Missi, and underestimation for Juá and Irauçuba, agreeing with the findings of Shrestha et al. (2017) and Silva et al. (2020a). In a similar validation study of CHIRPS data in Brazil, Costa et al. (2019) reported an overestimation of 3% relative to INMET/CPTEC data, with a 97% coefficient of determination between the datasets. The Root Mean Square Error (REQM) of the CHIRPS data ranged from 12.05 mm/year to 28.03 mm/year, indicating differences of up to 28.03 mm/year compared to automatic weather station data. These findings are consistent with those of Costa et al. (2019), who validated CHIRPS data using 64 weather stations in the Northeast region of Brazil.

Table 7. Statistical analysis of parameters used for spatial validation of CHIRPS rainfall.

Weather Stations	*R*	BP	REQM (mm/year)	*Willmott*	Elevation (m)
Missi	0.82	6.20	26.84	0.99	99
Juá	0.84	-20.00	12.05	0.95	180
Irauçuba	0.90	-26.41	28.03	0.92	190

Where: R^2- coefficients of determination; r - Pearson Correlation Coefficient; BP - Percentage Bias; $REQM$ -Square Root of the Mean Error.

Willmott's concordance index ranged from 0.92 to 0.99 (Figure 4 and Table 7), indicating a high level of accuracy in the CHIRPS rainfall data. Azevedo et al. (2020) also found acceptable accuracy ranges (0.81-0.94) for rainfall data in the Piranhas-Açú river basin, Rio Grande do Norte section.

The combined observations for issi, Juá, and Irauçuba related to rainfall estimates using CHIRPS yielded an r-value of 0.89, BP of -13.40 mm/year, $REQM$ of 22.31 mm/year, and a Willmott index of 0.98. These results indicate the suitability of CHIRPS data for environmental studies at various scales and suggest a good correlation between CHIRPS data and field weather station measurements (Hinrichs et al., 2019).

The historical evolution of land use and land cover in the Municipality of Irauçuba, Ceará, Brazil, is presented in Figure 5. The maps identify and evaluate land covers, such as forests, non-forest natural formations, agriculture, non-vegetated areas, and water bodies (MapBiomas, 2022). The map demonstrates how land use and cover have transformed over the years, offering insights for environmental and land management studies.

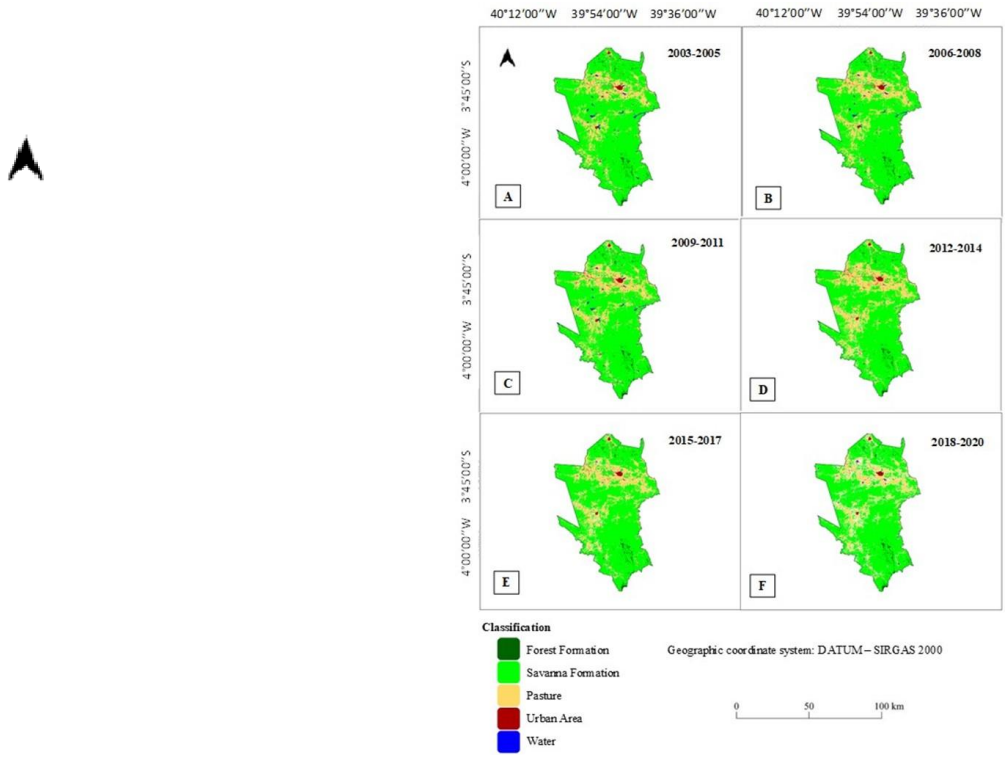

Figure 5. Temporal changes in land use and land cover in the municipality of Irauçuba, Ceará, Brazil from 2003 to 2020. Source: Own.

Land use for agricultural activity has changed over time in the municipality of Irauçuba. Agricultural activities peaked between 2012 and 2014 (Figure 5D) and the minimum between 2003 and 2005 (Figure 5A). It is worth noting that the management of agricultural activities by the municipality plays a crucial role in the process of desertification. For decades, cattle, goat, and sheep herds have been exerting significant pressure on the grazing lands. According to IBGE (2021) data, the number of bovines in Irauçuba has significantly decreased from 2004 to 2021, with only 13,548 heads reported in 2021. The goat herd remained stable, with 8,919 goats in 2004, 11,461 in 2012, and 10,024 in 2021. The sheep herd has increased, with 19,315 head of sheep in 2004, 26,426 in 2012, and falling to 22,356 in 2021. However, these animals still represent the largest herd in the region. These statistics demonstrate a shift from cattle to goat and sheep herding in the municipality, leading to land degradation. The grazing process of these animals is more intense than that of cattle, and they tend to remove all the vegetation, hindering regeneration and leaving the soil exposed (Araújo et al., 2015).

The number of agricultural establishments in Irauçuba has grown from 1,466 in 2006 to 2,100 in 2017. However, this expansion has hurt the soil due to plantations being implemented on slopes during rainy periods, leading to erosion (IBGE, 2022; Araújo Filho and Silva, 2010). Deforestation is another significant contributor to soil degradation in the region, decreasing biodiversity and leaving the soil exposed to erosion (Silva and Pacheco, 2016). These effects are visible in the reduction of the original area and expansion of the regions dedicated to economic activities, as observed in Figures 5A and 5D.

In water bodies, the highest average of 17.43 km² was observed between 2003 and 2005 (Figure 5A), while the lowest of 1.93 km² between 2015 and 2017 (Figure 5E). The native forest areas also varied, with the highest average of 1181.35 km² observed between 2003 and 2005 (Figure 5A) and the lowest of 1072.70 km² observed between 2012 and 2014 (Figure 5D). The highest average occupation of non-vegetated areas was observed between 2012 and 2014 (Figure 5D), with 39.26 km², while the lowest was between 2018 and 2020 (Figure 5F). However, over the years, the Municipality of Irauçuba has been expanding its urbanized spaces and agricultural exploitation areas, replacing native forests with areas of human activity. Silva (2016) points out that this scenario resulted in nonproductive areas and increased environmental degradation. Sousa et al (2023) assert that this increase in the native vegetation areas may be related to the severe drought that occurred in the region between the years 2012 and 2015.

Table 8 presents the r and R^2 coefficient values for LST, NDVI, and CHIRPS data. Remarkably, most products showed a negative correlation, except for NDVI and CHIRPS data. The strongest correlation was found between NDVI and CHIRPS data (r = 0.928), whereas the weakest was between LST and NDVI (r = -0.972). Furthermore, the highest R^2 coefficient was observed between LST and NDVI (R^2 = 0.946), indicating a robust relationship between these parameters. It's worth emphasizing that the variation in LST is related to water deficit, an indicator of water stress in the area. Overall, these results suggest that the studied biophysical parameters are strongly interdependent and can provide valuable insights for monitoring environmental conditions in the region.

Table 8. Correlation Analysis between LST, NDVI, and CHIRPS data. Source: Own.

Parameter relations	r	R^2
LST X NDVI	-0.972	0.946
LST X CHIRPS	-0.824	0.679
NDVI X CHIRPS	0.928	0.862

Figure 6 presents a visual representation of the average NDVI values over time, allowing the observation of changes in vegetation cover in the study area between 2003 and 2020. This graph serves as a tool to identify patterns and trends in the data, providing information about the state of vegetation cover in the region.

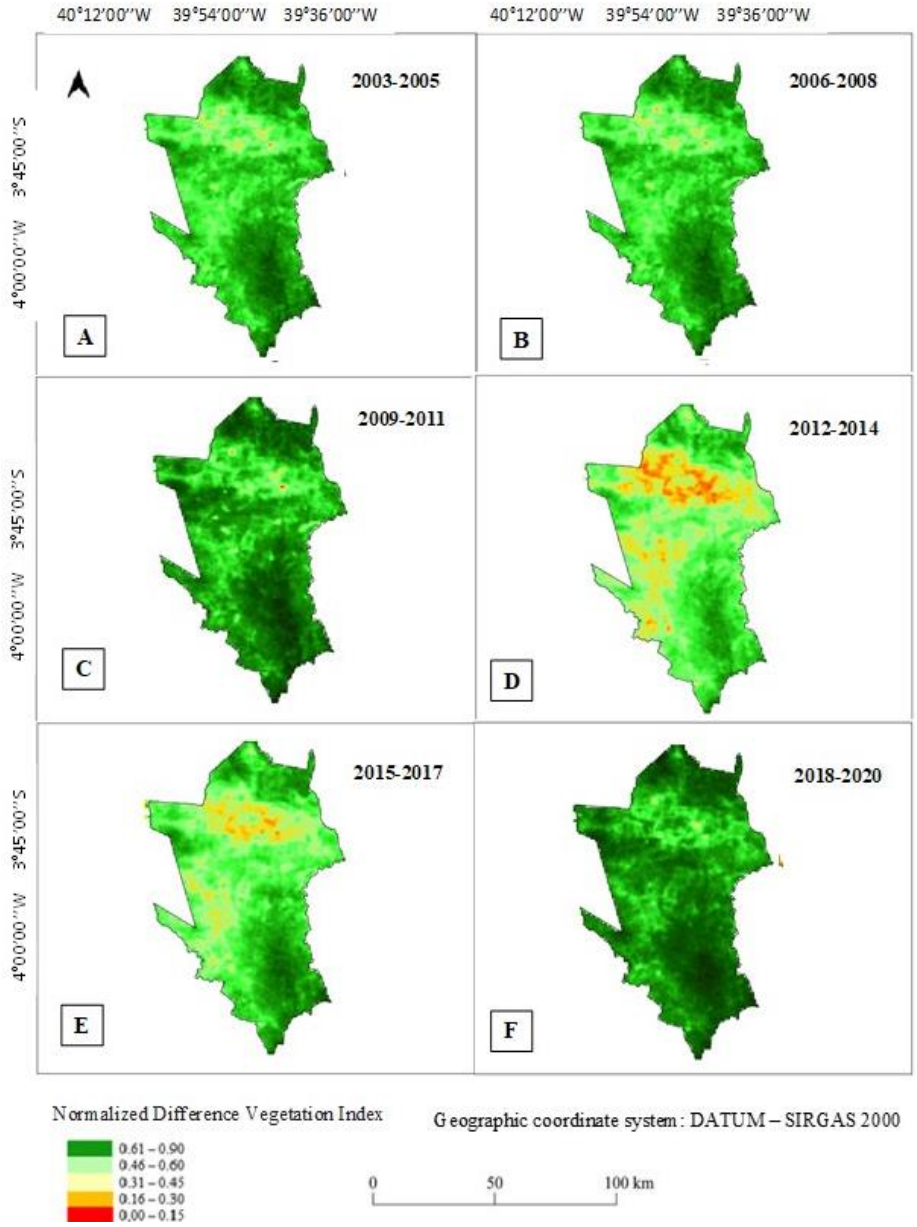

Figure 6. Spatial distribution of Normalized Difference Vegetation Index (NDVI) from 2003 to 2020. Source: Own.

The highest NDVI values were observed from 2018 to 2020 (Figure 6F), attributed to increased rainfall in the municipality. In contrast, the period from 2012 to 2014 (Figure 6D) had the lowest NDVI values, likely due to the removal of vegetation cover for various purposes, according to Santos et al. (2014). It is worth noting that vegetation vigor decay was less severe from 2003 to 2005 (Figure 6A), although 2005 had the second highest negative value of RAI, as shown in Figure 3. On the other hand, the period from 2015 to 2017 (Figure 6E) had more negative RAI values than 2005 and exhibited a decline in vegetation vigor. Thus, a single year of drought may have less impact on the vegetation of the caatinga biome than several consecutive years. These findings have implications for controlling environmental degradation and desertification in the municipality of Irauçuba. The results of this study identify vulnerable areas and will help decision-making processes related to environmental conservation and land use planning.

Notably, a strong positive correlation was observed between the NDVI and CHIRPS data, as also observed by previous studies by Landim, Silva, and Almeida (2011) and Santos et al. (2014) on vegetation in the municipality of Irauçuba. This relationship suggests that changes in rainfall

patterns impact vegetation cover, emphasizing the importance of monitoring both variables to understand environmental changes in the region.

Figure 7 shows the mean annual rainfall for the study area over the past 17 years. There were rainfall increases from west to east and low concentrations in the central parts of the municipality. The spatial distribution map illustrates a direct relationship between maximum annual rainfall, vegetation cover, and topography. It also reveals that places in the southeast of the municipality had high rainfall concentrations, even in periods of drought. In the southeast of the area, rainfall concentrations are high, even in periods of drought. This portion of the region has high elevations, resulting in low average air temperatures and increased rainfall due to orographic effects (Lima et al., 2022).

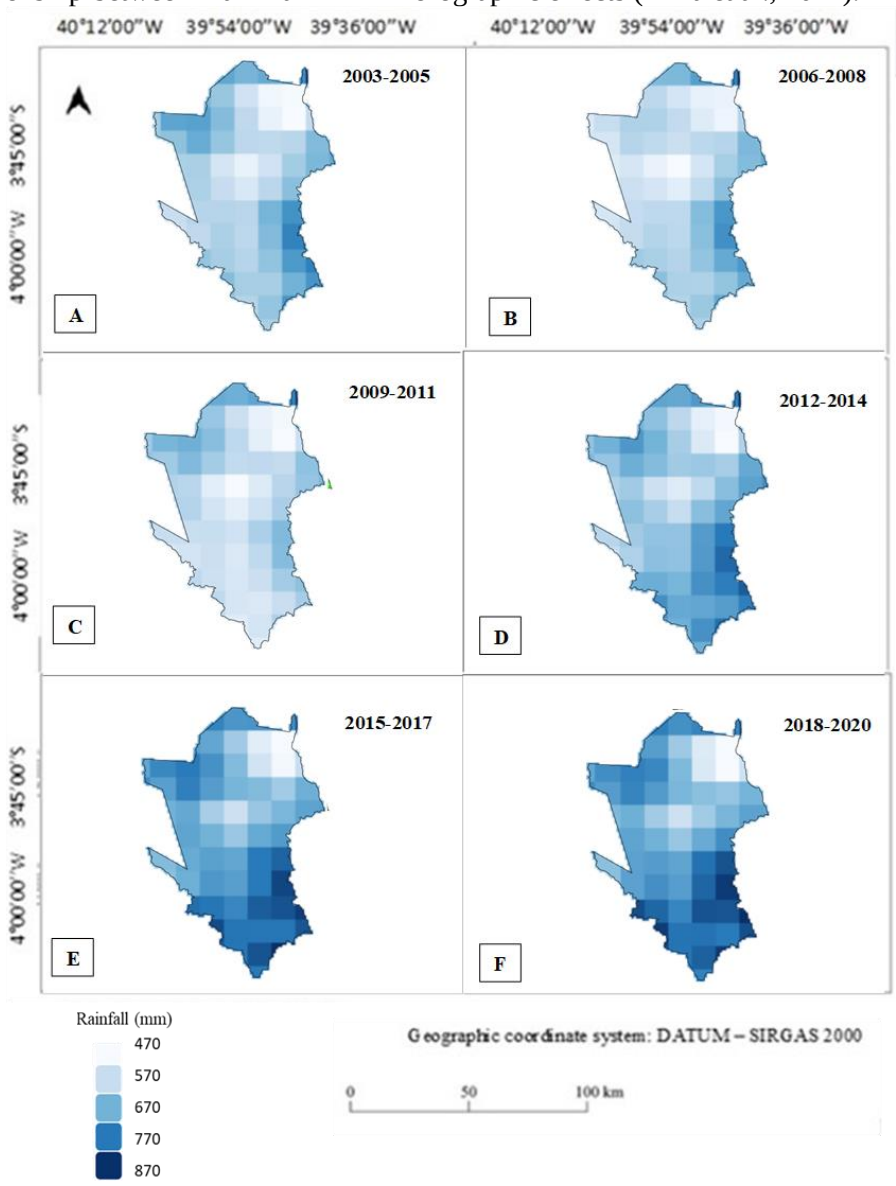

Figure 7. Spatial distribution of mean annual rainfall using CHIRPS data from 2003 to 2020. Source: Own.

Table 9 shows that the highest average rainfall was recorded from 2018 to 2020, with a total of 847.83 mm, while the lowest occurred from 2012 to 2014, with a total of 452.59 mm. The standard deviation of rainfall ranged from 50.13 to 101.15 mm. These findings are consistent with the results of Lima et al. (2022), who used CHIRPS data to analyze rainfall patterns in the Ibiapaba region of Northeastern Brazil, reporting similar cumulative rainfall values for 2018, 2019, and 2020 compared to other years.

Table 9. Statistical Parameters of rainfall (CHIRPS data) for the study area from 2003 to 2020.

Years	Rainfall (mm)			
	Max	**Mean**	**Min**	**SD**
2003-2005	904.55	619.27	461.86	71.17
2006-2008	924.08	605.10	465.07	67.45
2009-2011	1098.63	718.95	580.33	69.54
2012-2014	609.32	452.59	329.52	50.13
2015-2017	760.84	611.87	415.07	73.75
2018-2020	1038.75	847.83	586.03	101.15

Where: Max: Maximum; Min: Minimum; SD: Standard Deviation.

Figure 8 corresponds to the potential evapotranspiration (PET) images over the study area. The lowest PET average was observed from 2006 to 2008 (Figure 8B), with a value of 1784.75 mm, while the highest PET average was 1899.92 mm from 2003 to 2005 (Figure 8A).

The period from 2003 to 2005 (Figure 8A) were the highest evapotranspiration rate, while the period from 2012 to 2014 (Figure 8D) had the lowest rate, with 2370.37 mm and 930.83 mm, respectively. These observations suggest that PET in the study area varies significantly over time.

Table 10 presents PET statistics in the study area from 2003 to 2020. The standard deviation of PET values ranged from 119.77 to 217.46 mm.

The spatial variability in PET values is related to differences in vegetation cover, soil type, and topography. Despite these variations, there was no significant relationship between PET and other biophysical data (Viana et al., 2013). This lack of correlation is related to the time lag in perceiving the effect of the coverage-rainfall-evapotranspiration relationship

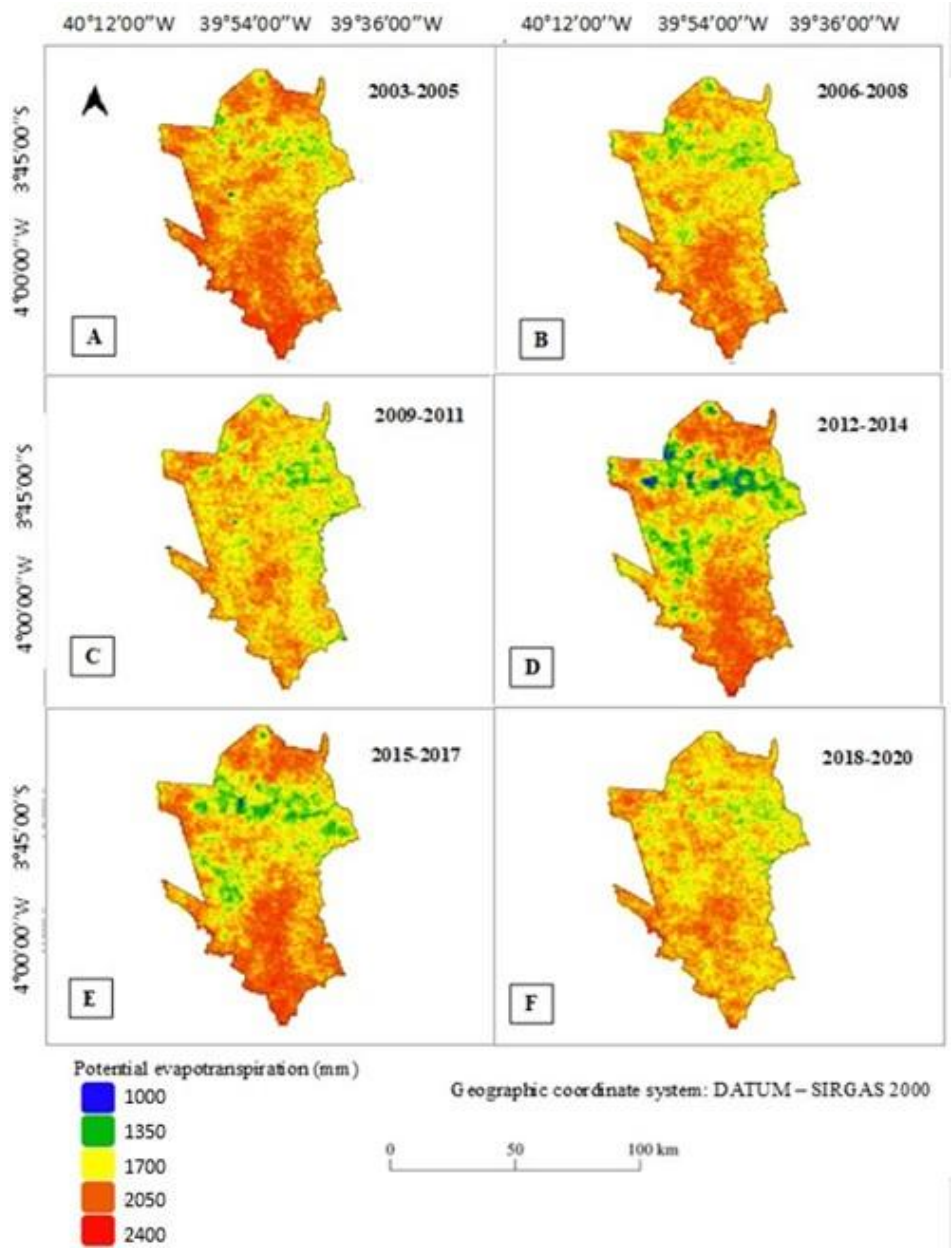

Figure 8. Spatial distribution of potential evapotranspiration using MODIS product (MOD16A2) from 2003–2020. Source: Own.

Table 10. Statistical of potential evapotranspiration (PET) during 2003 to 2020.

Years	PET (mm)			
	Max	**Mean**	**Min**	**SD**
2003-2005	2370.37	1899.92	1028.93	158.00
2006-2008	2233.33	1822.03	1221.23	153.50
2009-2011	2184.23	1784.75	115193	134.33
2012-2014	2353.77	1801.88	930.83	217.46
2015-2017	2359.00	1834.04	947.73	193.78
2018-2020	2236.13	1814.00	1403.43	119.77

Where: Min - Minimum; Max - Maximum; SD - Standard Deviation.

Figure 9 shows the Land Surface Temperature (LST) images over the study area. LST showed an inverse correlation with NDVI values and CHIRPS data (Table 7). The highest LST value over the study area was 244.05 K observed from 2012 to 2014 (Figure 9D). However, it is noteworthy that the average temperature did not vary significantly across all periods. The standard deviation ranged from 97.46 to 119.06, indicating relatively low variability in LST values. Santos et al. (2014) established a correlation between temperature increase and vegetation removal for various purposes, resulting in significant landscape alteration in the region. This finding is consistent with the observation by Aragão et al. (2007), who noted that forest conversion for other uses such as agriculture, livestock, and logging, which leave large portions of soil exposed, are directly associated with the temperature rise. Neto et al (2023) agreed that the deforestation and fires tied to land occupation by agriculture are determinant for changes in the local climate, increasing temperature and reducing relative air humidity and rainfall indexes.

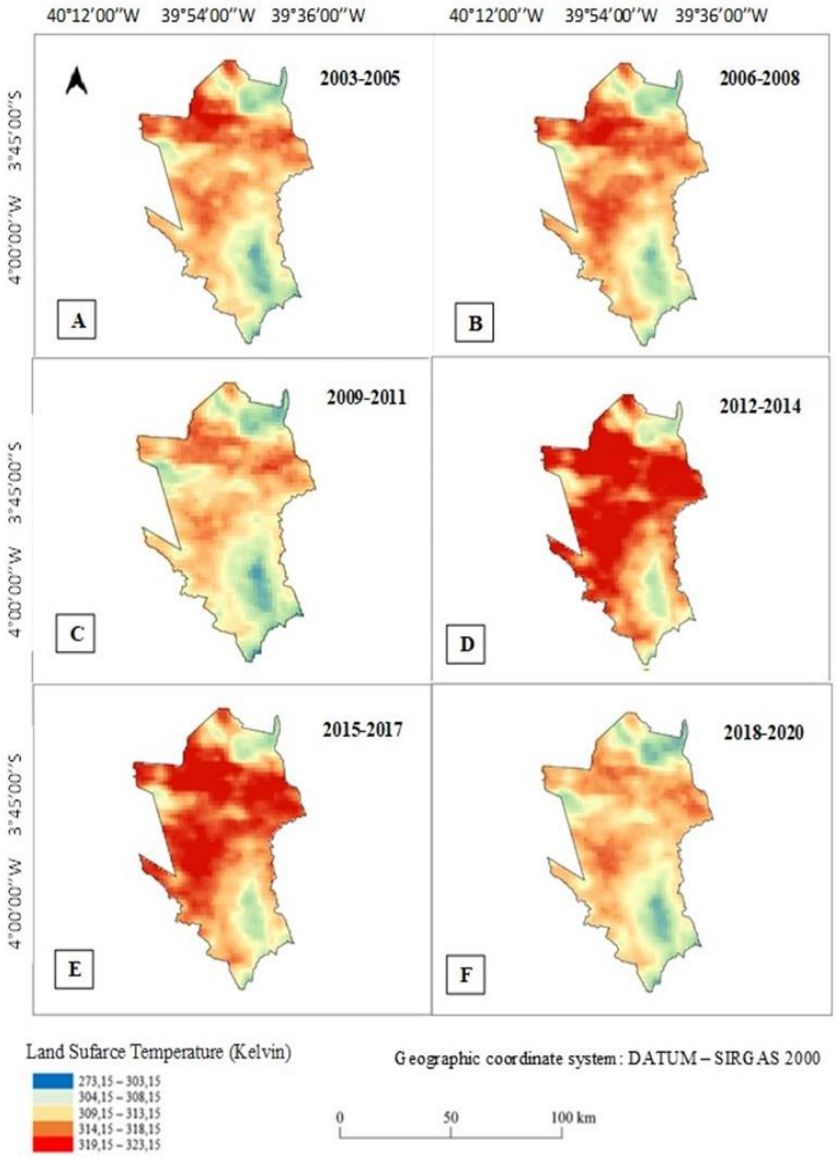

Figure 9. Spatial distribution of Land surface temperature using MODIS product (MOD11A2) from 2003 to 2020. Source: Own.

Figure 10 and Table 11 show the results of the aridity index, climate classification, and level of susceptibility to desertification calculated from CHIRPS data and MODIS potential evapotranspiration for the period from 2003 to 2020 in the municipality of Irauçuba. The aridity

index (AI) varied between the six periods, with values between 0.255 and 0.464. The highest AI was observed from 2018 to 2020 (Figure 10F), while the lowest from 2012 to 2014 (Figure 10D). The climate classification of the six periods analyzed was semiarid. In addition, the Desertification Susceptibility Level (NS) was high in all years. These findings are consistent with previous studies conducted by Vilar and Medeiros (2019) and França et al. (2020a) in Pernambuco, and França et al. (2020b) in Sergipe.

Table 11. Aridity Index (AI), Climate Classification (CC), and Susceptibility Level (SL) from 2003 to 2020.

Periods	AI	CC	SL
2003-2005	0.322	Semiarid	High
2006-2008	0.330	Semiarid	High
2009-2011	0.409	Semiarid	High
2012-2014	0.255	Semiarid	High
2015-2017	0.334	Semiarid	High
2018-2020	0.464	Semiarid	High

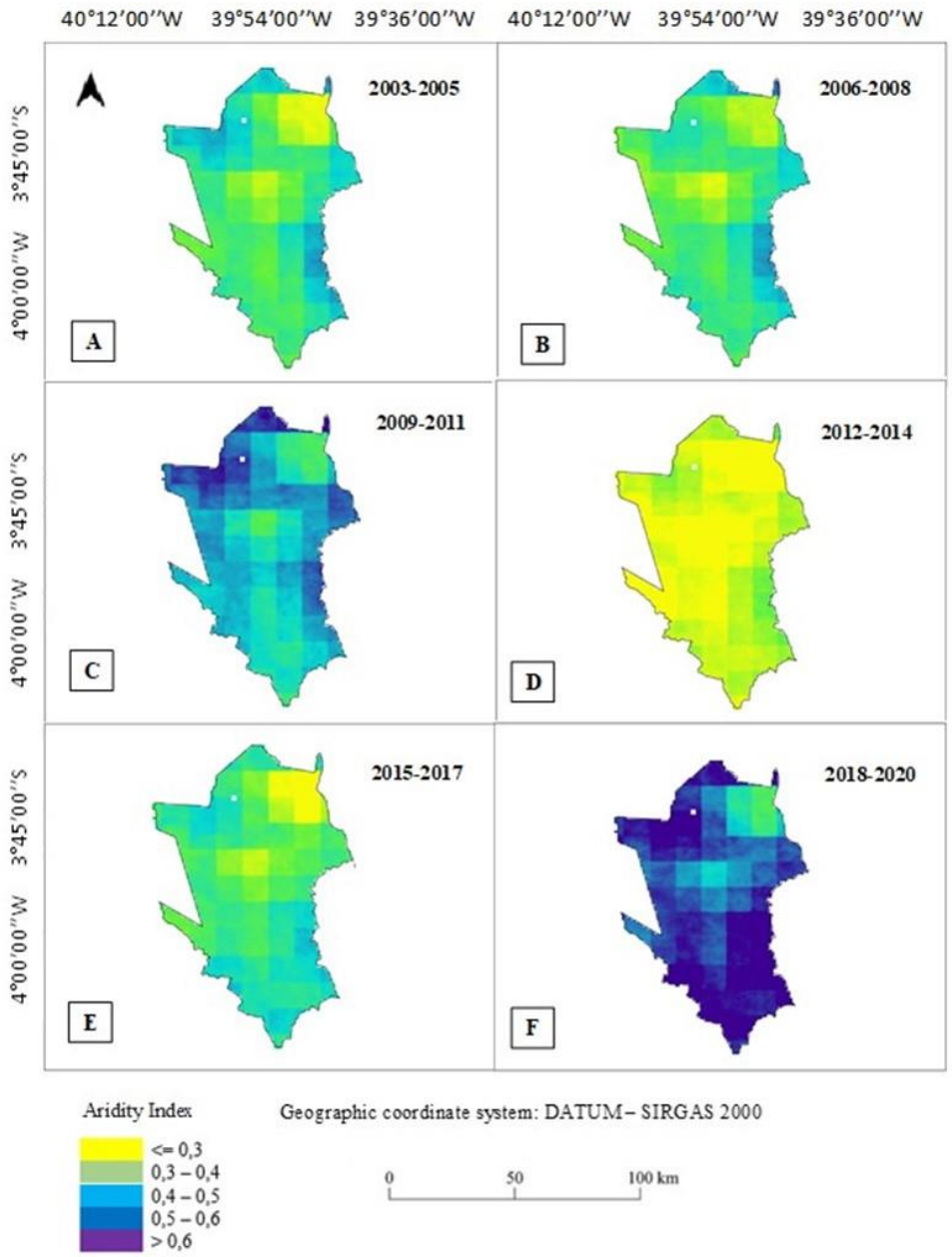

Figure 10. Spatial distribution of the Aridity Index using CHIRPS data and MODIS products (MOD16A2) from 2003 to 2020. Source: Own.

Conclusion

The phenotypic techniques adopted to characterize *Paspalum* accessions demonstrate useful to evaluate their use on simulated green roofs. The accessions of upright growth habit provide the better results and potential to be use in green roofs for thermal comfort

The SAVI index can be used to estimate the coverage capacity (CC), and to identifying how much of this coverage is the green matter (MG%) and dry matter (MD%), characteristics of great relevance in the selection of lawns for green roofs, associated with aspects of establishment, persistence, resilience, and resistance.

Leaf and canopy temperatures can be used as an indication of water deficit in *Paspalum* accessions, using both the infrared thermometer, whose equipment is more accessible, and the thermographic camera.

Canopy temperatures can also be used to evaluate the plant functionality to reduce the temperature on the roof, minimizing the temperature of the environments. Higher plants present lower canopy temperatures as observed in accessions of Paspalum with upright growth habit. We recommend that further studies to select *Paspalum* accessions for use on green roofs be carried with different soil and climatic conditions.

Acknowledgment

To the *Programa de Pós-Graduação em Agronomia – Melhoramento Genético de Planta* and the *Grupo de Pesquisa em Floricultura e Paisagismo da Universidade Federal Rural de Pernambuco* (UFRPE) for supporting the development of this research. To the *Conselho Nacional de Desenvolvimento Científico e Tecnológico* (CNPq) for funding the scholarship.

References

Abdulridha, J.,Batuman, O., & Ampatzidis, Y. 2019a. UAV-Based Remote Sensing Technique to Detect Citrus Canker Disease Utilizing Hyperspectral Imaging and Machine Learning. Remote Sens, 11 (11), 1373. https://doi.org/10.3390/rs11111373

Abdulridha, J., Ehsani, R., Abd-Elrahman, A., & Ampatzidis, Y. 2019b. A remote sensing technique for detecting laurel wilt disease in avocado in presence of other biotic and abiotic stresses. Computers and electronics in agriculture, 156, 549-557. https://doi.org/10.1016/j.compag.2018.12.018.

Amorim, M. C. D. C. T. 2019. Ilhas de calor urbanas: métodos e técnicas de análise. Revista Brasileira de Climatologia, 22-46. DOI: http://dx.doi.org/10.5380/abclima.v0i0.

Alvarenga, C. B., Teixeira, M. M., Zolnier, S., Sasaki, R. S., & Rinaldi, P. C. N. 2013. Controle automático do espectro de gotas de pulverizador hidropneumático em função do déficit de pressão de vapor d'água no ar. Pesquisa Agropecuária Tropical, 43(1), 26-33. https://doi.org/10.1590/S1983-40632013000100006.

Ampatzidis, Y., De Bellis, L., & Luvisi, A. 2017. iPathology: robotic applications and management of plants and plant diseases. Sustainability, 9(6), 1010. https://doi.org/10.3390/su9061010

Carvalho, I. D. E., Ferreira, P. V., Pereira, M. G., da Silva Neto, J. V., da Silva Júnior, A. B., dos Santos Ferreira, D., & Pereira, C. C. A. 2019. Evaluation of Melon Plant Grown in Saline Environment. Journal of Experimental Agriculture International, 1-14. https://doi.org/10.9734/jeai/2019/v37i430273.

Caturegli, L., Grossi, N., Saltari, M., Gaetani, M., Magni, S., Nikolopoulou, A. E., ... & Volterrani, M. 2015. Spectral reflectance of tall fescue (Festuca arundinacea Schreb.) under different irrigation and nitrogen conditions. Agriculture and Agricultural Science Procedia, 4, 59-67. https://doi.org/10.1016/j.aaspro.2015.03.008.

Costa, A. P. L. 2020. Fenotipagem de precisão na cultura do amendoim para detecção de déficit hídrico. South American Sciences, 1(2), e2064. http://dx.doi.org/10.17648/sas.v1i2.64.

Costa, N. D. L., Magalhães, J. A., Townsend, C. R., & Paulino, V. T. 2004. Fisiologia e manejo de plantas forrageiras. Embrapa Rondônia-Documentos (INFOTECA-E). Recuperado em 16 de julho, 2020, de https://www.infoteca.cnptia.embrapa.br/infoteca/handle/doc/916005.

EOS – EARTH OBSERVING SYSTEM. 2019. NDVI FAQ: All you need to know about NDVI. Retrieved May 15, 2020, from: https://eos.com/blog/ndvi-faq-all-you-need-to-know-about-ndvi/.

Ferrante, P., La Gennusa, M., Peri, G., Rizzo, G., & Scaccianoce, G. 2016. Vegetation growth parameters and leaf temperature: Experimental results from a six plots green roofs' system. Energy, 115, 1723-1732. https://doi.org/10.1016/j.energy.2016.07.085.

Ferreira, D. F. (2011). Sisvar: a computer statistical analysis system. Ciência e agrotecnologia, 35(6), 1039-1042. https://doi.org/10.1590/S1413-70542011000600001.

Fritsche-Neto, R., & Borém, A. (Eds.). 2015. Fenômica: como a fenotipagem de próxima geração está revolucionando o melhoramento de plantas. Viçosa: UFV.

Gameiro S., Teixeira C.P.B., Silva Neto T.A.S.; Lopes M.F.L., Duarte C.R., Souto M.V.S., Zimback C.R.L. 2016.Avaliação da cobertura vegetal por meio de índices de vegetação (NDVI, SAVI e IAF) na Sub-Bacia Hidrográfica do Baixo Jaguaribe, CE. Terræ, 13(1-2), 15-22. ISSN: 1679-2297.

Golzarian, M. R., & Frick, R. A. 2011. Classification of images of wheat, ryegrass and brome grass species at early growth stages using principal component analysis. Plant Methods, 7(1), 1-11. https://doi.org/10.1186/1746-4811-7-28.

Hackl, H., Baresel, J. P., Mistele, B., Hu, Y., & Schmidhalter, U. 2012. A comparison of plant temperatures as measured by thermal imaging and infrared thermometry. Journal of agronomy and crop science, 198(6), 415-429. https://doi.org/10.1111/j.1439-037X.2012.00512.x.

Huete, A.R 1988. A soil-adjusted vegetation index (SAVI). Remote sensing of environment, 25(3), 295-309. DOI: https://doi.org/10.1016/0034-4257(88)90106-X.

Ignatieva, M., Ahrné, K., Wissman, J., Eriksson, T., Tidåker, P., Hedblom, M., ... & Bengtsson, J. 2015 Lawn as a cultural and ecological phenomenon: a conceptual framework for transdisciplinary research. Urban Forestry & Urban Greening, 14(2), 383-387. DOI: https://doi.org/10.1016/j.ufug.2015.04.003.

Koyama, T., Yoshinaga, M., Hayashi, H., Maeda, K. I., & Yamauchi, A. 2013. Identification of key plant traits contributing to the cooling effects of green façades using freestanding walls. Building and Environment, 66, 96-103. DOI: https://doi.org/10.1016/j.buildenv.2013.04.020.

Krebs, L., Johansson, E., Krebs, C., Fedrizzi, B., & Grala da Cunha, E. 2017. Influence of extensive green roofs to the local microclimate: Cooling assessment for a social housing project in the South of Brazil. Proceedings of PLEA 2017 Edinburg: Design to thrive, 2, 2880-2887.

Li, L., Zhang, Q., & Huang, D. 2014. A review of imaging techniques for plant phenotyping. Sensors, 14(11), 20078-20111. DOI: https://doi.org/10.3390/s141120078.

Liz, D. S.,Ordenes, M., Guths ,S.2018. Análise experimental do comportamento término do telhado verde extensivo para Florianópolis. Revista Oculum Ensaios**,** 15(2). 315-333. DOI: https://doi.org/10.24220/2318-0919v15n2a4053.

Lopes, P.M.O., Valeriano, D. M., Silva, B. B., Moura, G A., & da Silva, A. O. 2013 Simulation of net radiation in the Mantiqueira mountain. Revista Brasileira de Engenharia Agrícola ambiental. 17 (7), p.780-789. https://doi.org/10.1590/S1415-43662013000700013

Lundholm, J., Tran, S., & Gebert, L. 2015. Plant functional traits predict green roof ecosystem services. Environmental science & technology, 49(4), 2366-2374. https://doi.org/10.1021/es505426z.

Neto., A. M., Fernandes, G. S. T., Lima, E. A. Lopes, P. M. O., Rodrigues, L. A. Junior, A. S. G., Lopes., J. R. A., Silva, L. L. S., Silva., R. O. 2023. Evapotranspiration in the context of land use and land cover changes in MATOPIBA, Brazil; A theoretical approach. Revista Brasileira de Geografia Física v.16, n.01, 050-062. DOI: https://doi.org/10.26848/rbgf.v16.1.p050-062

Martínez, J., Egea, G., Agüera, J., & Pérez-Ruiz, M. 2017. A cost-effective canopy temperature measurement system for precision agriculture: a case study on sugar beet. Precision Agriculture, 18(1), 95-110. https://doi.org/10.1007/s11119-016-9470-9.

Monteiro, M. V., Blanuša, T., Verhoef, A., Richardson, M., Hadley, P., & Cameron, R. W. F. 2017. Functional green roofs: Importance of plant choice in maximising summertime environmental cooling and substrate insulation potential. Energy and buildings, 141, 56-68. https://doi.org/10.1016/j.enbuild.2017.02.011.

Peng, J., Hu, Y., Dong, J., Liu, Q., & Liu, Y. 2020. Quantifying spatial morphology and connectivity of urban heat islands in a megacity: A radius approach. Science of The Total Environment, 714, 136792. https://doi.org/10.1016/j.scitotenv.2020.136792.

Pesck, A. 2017. Uso de NDVI e SAVI para Caracterização da Cobertura da Terra e Análise Temporal em Imagens RapidEye. Revista ESPACIOS, 38 (36),7-21. ISSN 0798 1015.

Pires, W. N., de Moura, M. S. B., Aidar, S. D. T., & de Souza, L. S. B. 2015, maio). Temperatura

foliar e do dossel como indicador de déficit hídrico em plantas da Caatinga: resultados iniciais. In Anais do IV Simpósio de Mudanças Climáticas e Desertificação no Semiárido Brasileiro, Petrolina, PE.

Ponzoni, F. J.. 2001. Comportamento espectral da vegetação. Sensoriamento remoto: reflectância de alvos naturais. Brasília: UNB.

Potgieter, A. B., Watson, J., George-Jaeggli, B., McLean, G., Eldridge, M., Chapman, S. C., ... & Jordan, D. R. 2018. The use of hyperspectral proximal sensing for phenotyping of plant breeding trials. In Fundamentals, Sensor Systems, Spectral Libraries, and Data Mining for Vegetation (pp. 127-147). CRC Press.

Rouse Jr, J. W., Haas, R. H., Deering, D. W., & Schell, J. A. 1973. Monitoring the vernal advancement and retrogradation (Green Wave Effect) of natural vegetation.[Great Plains Corridor].

Santos, S. M., Silva, J. F. F., dos Santos, G. C., de Macedo, P. M. T., & Gavazza, S. 2019. Integrating conventional and green roofs for mitigating thermal discomfort and water scarcity in urban areas. Journal of Cleaner Production, 219, 639-648. https://doi.org/10.1016/j.jclepro.2019.01.068.

Silva, S. Á. C. G. D., Albuquerque, J. C. C. D., Silva, S. S. L., Castro, A. C. R. D., & Loges, V. 2020. Development of Paspalum accession plugs for turfgrass establishment. Ornamental Horticulture, 26, 356-366. https://doi.org/10.1590/2447-536X.v26i3.2163.

Silva, S. Á., Santos, A. G., Silva, S. S. L., Loges, V., de Souza, F. H. D., & Castro, A. C.2018. Characterization and selection of Brazilian native grasses for use as turfgrass. Acta Horticulturae, (1215), 255-258. ISSN: 0567-7572.

Silva, V.S., Salami, G., da Silva, M.I.O., Silva, E.A., Monteiro Junior, J.J., & Alba, E. (2020). Methodological evaluation of vegetation indexes in land use and land cover (LULC) classification. Geology, Ecology, and Landscapes, 4(2), 159-169. https://doi.org/10.1080/24749508.2019.1608409.

Silveira, L. P., Piuzana, D., Pereira, I. M , M. L. R., & Santos, J. B. 2016. Estimativa da cobertura de gramíneas invasoras em área degradada de cerrado por meio do Software Imagej. Revista ESPACIOS, 37 (31), 26. ISSN: 0798-1015.

Simões, C. R., Rossiello, R. O. P., Graciosa, M. G., Machado, M. L., & Silva, C. F. D. 2015. Imagens multiespectrais para avaliação de índice de área foliar e massa seca do capim'Tifton 85', sob adubação nitrogenada. Ciência Rural, 45(4), 697-703. http://dx.doi.org/10.1590/0103-8478cr20131424.

Sousa, C. A. F. 2014. Fenotipagem de plantas: uma nova abordagem para um velho problema. Embrapa Agroenergia-Comunicado Técnico (INFOTECA-E).

Sousa, C. A. F., da Cunha, B. A. D. B., Martins, P. K., Correa, H. B., Molinari, A. K. K., & Júnior, M. T. S. 2015. Nova abordagem para a fenotipagem de plantas: conceitos, ferramentas e perspectivas. Rev. Bras. Geogr. Física, 8 (IV SMUD), 660-672. https://doi.org/10.26848/rbgf.v8.0.p660-672.

Souza, F. H. D., Gusmão, M. R., Matta, F. D. P., Castro, A. C. R., Mittelmann, A., Fávero, A. P., & Jank, L. 2016. Atributos desejáveis para gramados a serem cultivados sob condições brasileiras: uma proposta. Ornamental Horticulture, 22(2), 54-165. https://doi.org/10.14295/oh.v22i2.841.

Souza, H. B., Baio, F. H., & Neves, D. C. 2017. Using passive and active multispectral sensors on the correlation with the phenological indices of cotton. Engenharia Agrícola, 37(4), 782-789. http://dx.doi.org/10.1590/1809-4430-eng.agric.v37n4p782-789/2017.

Sousa, L. d. B. d., Montenegro, A. A. d. A., Silva, M.V.d., Lopes, P.M.O., Silva, J.R.I., Silva, T. G. F. d., Lins, F.A.C., & Silva, P.C. 2023. Spatiotemporal Dynamics of Land Useand Land Cover throughPhysical–Hydraulic Indices: Insightsin the São Francisco RiverTransboundary Region, BrazilianSemiarid Area. AgriEngineering 2023,5, 1147–1162. https://doi.org/10.3390/agriengineering5030073

Tan, P. Y., & Sia, A. 2009. Understanding the performance of plants on non-irrigated green roofs in Singapore using a biomass yield approach. Nature in Singapore, 2, 149-153. ISSN: 2010-0515.

Tassi, R., Tassinari, L. C. D. S., Piccilli, D. G. A., & Persch, C. G. 2014. Telhado verde: uma alternativa sustentável para a gestão das águas pluviais. Ambiente Construído, 14, 139-154. ISSN: 1678-8621.

Tattaris, M., Reynolds, M. P., & Chapman, S. C. 2016. A direct comparison of remote sensing approaches for high-throughput phenotyping in

plant breeding. Frontiers in Plant Science, 7, 1131. https://doi.org/10.3389/fpls.2016.01131.

Tetens, O. 1930. Uber einige meteorologische Begriffe, Z. Geophys, 6, p. 297-309.

Wachowicz, C. M., & de Carvalho, R. I. N. 2002. Fisiologia vegetal: produção e pós-colheita. Curitiba: Champagnat.

White, J. W., Andrade-Sanchez, P., Gore, M. A., Bronson, K. F., Coffelt, T. A., Conley, M. M.,& Wang, G. 2012. Field-based phenomics for plant genetics research. Field Crops Research, 133, 101-112. https://doi.org/10.1016/j.fcr.2012.04.003.

Yu, L., Wang, W., Zhang, X., & Zheng, W. 2015, September. A review on leaf temperature sensor: Measurement methods and application. In International conference on computer and computing technologies in agriculture (pp. 216-230). Springer, Cham. https://doi.org/10.1007/978-3-319-48357-3_21OI: